Behavioral Modeling of Nonlinear RF Power Amplifiers Considering Memory Effects

Hyunchul Ku, *Student Member, IEEE,* and J. Stevenson Kenney, *Senior Member, IEEE*

***Abstract*—This paper proposes a new behavioral model to treat memory effects in nonlinear power amplifiers (PAs). Phenomena such as asymmetries in lower and upper intermodulation terms, and variation of AM/AM and AM/PM, depending on signal history, are often observed in high-power PAs. To treat these phenomena, this paper presents a model based on the previously developed memory polynomial model. The contribution made in this paper is to augment the memory polynomial model to include a sparse delay tap structure that reduces the parameter space required for accurate model identification. A figure-of-merit, called the memory effect ratio, is defined to quantify the relative level of distortion due to memory effects, as compared to the memoryless portion. Another figure-of-merit is defined as the memory effect modeling ratio, which quantifies the degree to which the PA memory effects have been accounted for in the model. This new technique is validated using a variety of RF PAs, including an 880-MHz and a 2.1-GHz high-power laterally diffused metal–oxide semiconductor PA and various signals such as two-tone, eight-tone, and IS-95B signals.**

***Index Terms*—Asymmetries, intermodulation, memory effect, memory polynomial, nonlinearities, power amplifiers (PAs).**

I. Introduction

AN ESSENTIAL first step in analyzing a power-amplifier (PA) system and designing a linearizer for a PA is to model the PA nonlinearity accurately. Behavioral modeling is often used in PA nonlinearity modeling because it provides a computationally efficient means by relating input and output signals without resorting to a physical analysis of a device or system. To obtain a behavioral model for a PA system, we measure the nonlinear behavior of a PA, and extract model parameters based on a predefined model architecture. This model is used as a mathematical description of the PA nonlinearity in the analysis of communication systems and in predistortion linearizer design.

There has been intensive research in memoryless nonlinear behavioral modeling of PAs based on AM/AM and AM/PM functions. These are static functions at a given temperature and dc bias. However, memory effects in real PAs often arise due to thermal effects and long time constants in dc-bias circuits. When we measure intermodulation distortion (IMD) to characterize the nonlinear behavior of a PA, asymmetries in lower and upper sidebands [1]–[4] and IMD magnitude variation depending on envelope frequency are often observed [3], [5]. This means that the AM/AM and AM/PM functions are not static, but change depending on the history of past input levels. It is known that these phenomena come from memory effects. Several studies have recently been conducted to deal with the asymmetric effect in PA nonlinearity [1]–[4]. In [1], Cripps explained the asymmetric effects using an envelope domain phase shift that depends on the amplitude distortion and its interaction with the AM/AM and AM/PM functions. Carvalho and Pedro [2] explained the reasons for IMD asymmetry by analyzing nonlinear circuit in small- and large- signal regions. They attribute the reasons to the terminating impedances at the baseband or difference frequencies. Vuolevi *et al.* [3] divided the memory effects into electrical and thermal memory effects, and attributed the reason for asymmetric IMD to the thermal memory effects. They suggested that the opposite phases of the thermal filter at the negative and positive envelope frequencies causes IMD power to add at one sideband, while subtracting at the other. Williams *et al.* [4] measured voltages and currents for IF and RF signals in the time domain and analyzed the asymmetric effects. Using an active load–pull setup, they showed the envelope termination affects asymmetrical effects. Several studies have also been conducted to treat dynamic AM/AM and AM/PM depending on history of past input levels [5]–[8]. Whatever reason may cause the asymmetric effects and variation of AM/AM and AM/PM depending on past input levels, a model to treat these phenomena is needed. In addition, if memory effects are not considered in a predistortion linearizer, there is limit to improvement in sideband reduction. To consider memory effects in a behavioral, two-box, or three-box model, which is a cascade connection of memoryless function and linear time invariant (LTI) filter(s), was suggested [9], [10]. Muha *et al.* [10] showed that a two-box model improve model fidelity for digitally modulated signal. However, Clark *et al.* [11] explained the problems in these models to capture real memory effects in a PA, and suggested a three-box model using two-tone dynamic AM/AM and AM/PM. In [5], a behavioral model that has a parallel Wiener structure was developed using a two-tone dynamic signal by the author.

In this paper, to treat the memory effects, a memory polynomial model with complex coefficients is used [12]. This model is similar with the parallel Wiener model in [5], but the delay tap filter is used instead of an infinite impulse response (IIR) filter, as in [5]. This structure provides a more efficient way to identify the parameters in the model with the linear matrix equation form. In addition, using the measured data in the time domain, the digitally modulated signal can be directly used to quantify the memory effects. A memory effect ratio (MER) is defined to quantify the amount of memory effects that may be attributed to the memory effects, relative to those produced by the memoryless portion. Additionally, a figure-of-merit,

Manuscript received April 16, 2003. This work was supported by Danam Communications Inc., San Jose, CA.

The authors are with the School of Electrical and Computer Engineering, Georgia Institute of Technology, Atlanta, GA 30332 USA (e-mail: gte661q@prism.gatech.edu; jskenney@ece.gatech.edu).

Digital Object Identifier 10.1109/TMTT.2003.820155

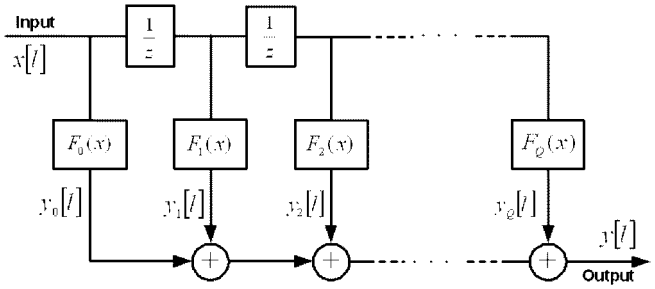

Fig. 1. PA model for a system with memory using a memory polynomial model with unit delay taps.

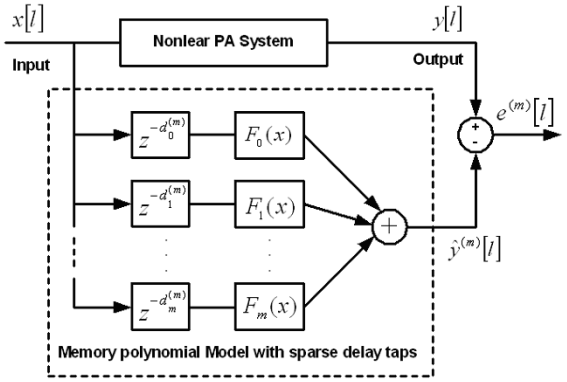

Fig. 2. PA model using a memory polynomial model with sparse delay taps.

which we call the memory effect modeling ratio (MEMR), is defined to quantify the effectiveness of the proposed model in accounting for all memory effects. Previously developed memory polynomial models used unit delay taps that result in a slow increase in the MEMR on a per-tap basis. We propose an improved memory polynomial model that uses sparse delay taps to improve the MEMR for the same number of parameters. For validation of the proposed model, many cases with various systems and various signals are investigated. First, two-tone output signals with significant IMD asymmetries are considered and modeled with the proposed model. Secondly, a 2.1-GHz 170-W peak envelope power (PEP) laterally diffused metal–oxide semiconductor (LDMOS) PA is measured with two-tone signals by sweeping input power and tone spacings, and subsequently modeled. Third, an 880-MHz 170-W PEP LDMOS PA is measured with eight-tone signals and modeled. Fourth, a sparse model with a finite number of delays is considered and modeled with an IS-95B signal. Finally, an 880-MHz 170-W PEP LDMOS PA is measured with an IS-95B signal and modeled. For each case, we extract MEMR values and compare those to show improvement of the suggested model.

II. PA Model Based on Memory Polynomial

A real or complex polynomial cannot describe IMD magnitude asymmetries, and represents only static AM/AM and AM/PM functions. In this section, a memory polynomial is considered to model the asymmetry and dynamic AM/AM and AM/PM. The memory polynomial that consists of several delay taps and nonlinear static functions is a truncation of the general Volterra series. It considers only diagonal terms in Volterra kernels, thus, the number of the parameters is significantly reduced compared to general Volterra series [12], [13]. The equivalent discrete baseband PA model considering memory effects and bandpass nonlinearity can be represented with a memory polynomial as follows:

$$y[l] = \sum_{q=0}^{Q} \sum_{k=1}^{n} a_{2k-1,q} \left| x[l-q] \right|^{2(k-1)} \cdot x[l-q] \qquad (1)$$

where $x[l]$ is the discrete input complex envelope signal and $y[l]$ is the discrete output complex envelope signal. This model considers only odd-order nonlinear terms due to bandpass nonlinear characteristics and the terms up to $2n-1$ are considered in modeling. The input signal, which has a delay of up to Q samples, is considered in this model. This model can be represented with a block model, as shown in Fig. 1. The structure of this model is similar to a finite impulse response (FIR) filter, but the difference is that polynomials $F_q(x)$ are used instead of the linear gain taps of an FIR filter. The function $F_q(x)$ can be represented with memoryless odd-order nonlinear functions such as

$$F_q(x) = \sum_{k=1}^{n} a_{2k-1,q} \left| x \right|^{2(k-1)} \cdot x. \qquad (2)$$

It was shown that this memory polynomial can model the memory effects in a PA [12], and the model can also be applied to predistortion linearizer [13]. However, to model the long-term memory effects, the model requires a large number of coefficients, even though it is small compared to a Volterra series, and shows a slow convergence of rms error between measured output and predicted output by adding delay taps. These problems can be improved by using sparse delay taps. The memory polynomial function with sparse delay taps is represented by

$$y[l] = \sum_{q=0}^{m} \sum_{k=1}^{n} a_{2k-1,q} \left| x\left[l - d_q^{(m)}\right] \right|^{2(k-1)} \cdot x\left[l - d_q^{(m)}\right] \qquad (3)$$

where $d_q^{(m)}$ is the sparse delay tap value when the number of the branches is $m+1$. The structure of a memory polynomial with sparse delay taps is shown in Fig. 2.

In order to extract the coefficients of the memoryless polynomial, and to get values of sparse delay taps, the memory polynomial function is represented by a matrix equation. From the measured input and output data in the time domain, we can define

$$\boldsymbol{Y} = \begin{bmatrix} y[l] & y[l+1] & \cdots & y[l+N-1] \end{bmatrix}^T \qquad (4)$$

and

$$\boldsymbol{H}^{(m)} = \begin{bmatrix} \boldsymbol{H}_0^{(m)} & \cdots & \boldsymbol{H}_q^{(m)} & \cdots & \boldsymbol{H}_m^{(m)} \end{bmatrix} \qquad (5)$$

where

$$\boldsymbol{H}_q^{(m)} = \begin{bmatrix} h_{1,q}^{(m)}[l] & h_{3,q}^{(m)}[l] & \cdots & h_{2n-1,q}^{(m)}[l] \\ h_{1,q}^{(m)}[l+1] & h_{3,q}^{(m)}[l+1] & \cdots & h_{2n-1,q}^{(m)}[l+1] \\ \vdots & \vdots & \ddots & \vdots \\ h_{1,q}^{(m)}[l+N-1] & h_{3,q}^{(m)}[l+N-1] & \cdots & h_{2n-1,q}^{(m)}[l+N-1] \end{bmatrix} \qquad (6)$$

and

$$h^{(m)}_{2k-1,q}[l] = \left|x\left[l-d^{(m)}_q\right]\right|^{2(k-1)} \cdot x\left[l-d^{(m)}_q\right]. \quad (7)$$

Let the complex coefficient be represented as follows:

$$\boldsymbol{a}^{(m)} = \left[\boldsymbol{a}^{(m)}_0 \quad \cdots \quad \boldsymbol{a}^{(m)}_q \quad \cdots \quad \boldsymbol{a}^{(m)}_m\right]^{\mathbf{T}} \quad (8)$$

where

$$\boldsymbol{a}^{(m)}_q = \left[a^{(m)}_{1,q} \quad a^{(m)}_{3,q} \quad \cdots \quad a^{(m)}_{2n-1,q}\right]. \quad (9)$$

Equation (3) with N consecutive time-domain data points can then be represented with a matrix equation such as

$$\boldsymbol{Y} = \boldsymbol{H}^{(m)} \cdot \boldsymbol{a}^{(m)} \quad (10)$$

where $\boldsymbol{Y}$ is an $N \times 1$ vector, $\boldsymbol{H}^{(m)}$ is an $N \times n(m+1)$ matrix, and $\boldsymbol{a}^{(m)}$ is an $n(m+1) \times 1$ vector. To get the coefficients that minimize rms error between the measured output and simulated output for the N consecutive measured time-domain data points, the expected coefficient set $\hat{\boldsymbol{a}}^{(m)}$ can be acquired using the following equation:

$$\hat{\boldsymbol{a}}^{(m)} = \left[\hat{\boldsymbol{a}}^{(m)}_0 \quad \cdots \quad \hat{\boldsymbol{a}}^{(m)}_q \quad \cdots \quad \hat{\boldsymbol{a}}^{(m)}_m\right]^{\boldsymbol{T}} = \boldsymbol{H}^{(m)^{-1}} \cdot \boldsymbol{Y} \quad (11)$$

where $\boldsymbol{H}^{(m)^{-1}}$ denotes the pseudoinverse matrix of $\boldsymbol{H}^{(m)}$. The expected output from the model is

$$\begin{aligned}\hat{\boldsymbol{Y}}^{(m)} &= \left[\hat{y}^{(m)}[l] \quad \hat{y}^{(m)}[l+1] \quad \cdots \quad \hat{y}^{(m)}[l+N-1]\right]^T \\ &= \boldsymbol{H}^{(m)} \cdot \hat{\boldsymbol{a}}^{(m)} = \sum_{q=0}^{m} \boldsymbol{H}^{(m)}_q \cdot \hat{\boldsymbol{a}}^{(m)}_q. \end{aligned} \quad (12)$$

The error between the measured and simulated data can be defined as

$$\begin{aligned}\boldsymbol{E}^{(m)} &= \boldsymbol{Y} - \hat{\boldsymbol{Y}}^{(m)} \\ &= \left[e^{(m)}[l] \quad e^{(m)}[l+1] \quad \cdots \quad e^{(m)}[l+N-1]\right]^T. \end{aligned} \quad (13)$$

In this case, the estimated rms error considering N consecutive time data points for the memory polynomial model with $m+1$ branches can be acquired as

$$\mathrm{rms}e[m] = \left(\frac{1}{N}\sum_{k=0}^{N-1}\left|e^{(m)}[l-k]\right|^2\right)^{1/2} = \frac{1}{\sqrt{N}}\left\|\mathbf{E}^{(m)}\right\|_2. \quad (14)$$

For a memoryless nonlinear application, m is set to 0 and $d^{(0)}_0$ is set to 0. For the memory polynomial model suggested in [12], the delay function $d^{(m)}_q$ is q. The block diagram to identify the proposed model for nonlinear RF PAs using the algorithms described in this section is shown in Fig. 3.

III. System Identification and Quantifying the Performance

For a memory polynomial with sparse delay taps, the optimal sparse delay tap can be represented with

$$\boldsymbol{d}^{(m)}_{\mathrm{opt}} = \left\{\boldsymbol{d}^{(m)} \middle| \min_{d^{(m)}}\left(\left\|\boldsymbol{E}^{(m)}\right\|^2_2\right), \boldsymbol{d}^{(m)} = \left\{d^{(m)}_0 \ldots d^{(m)}_m\right\}\right\} \quad (15)$$

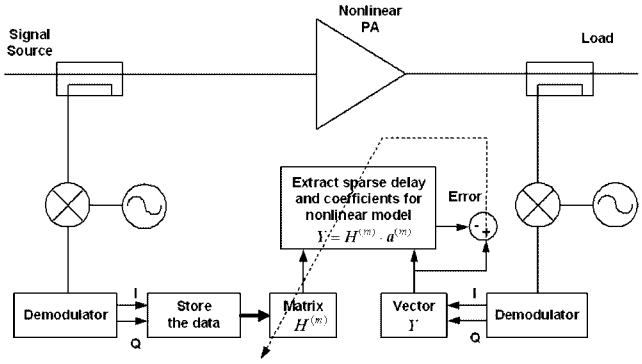

Fig. 3. Block diagram of the system identification procedure for the proposed model.

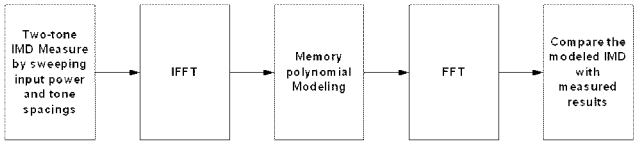

Fig. 4. Modeling procedure for two-tone or multitone frequency-domain data.

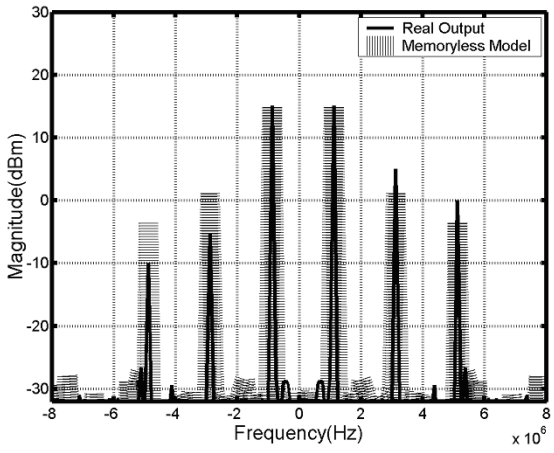

(a)

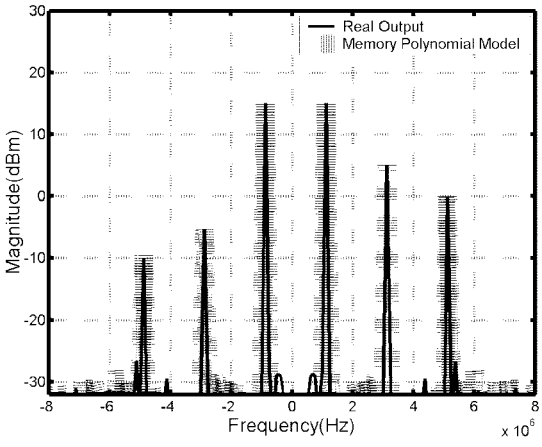

(b)

Fig. 5. Comparison of two-tone IMD in the frequency domain. (a) Memoryless model. (b) Model based on memory polynomial.

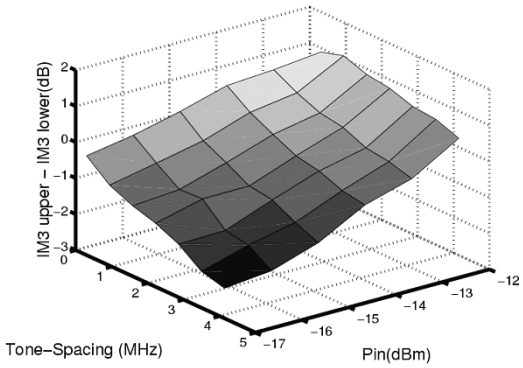

(a)

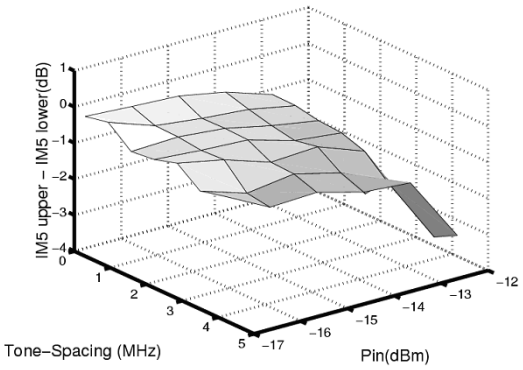

(b)

Fig. 6. Measured two-tone IMD asymmetries between upper and lower terms for a high-power LDMOS PA. (a) IMD3 asymmetries. (b) IMD5 asymmetries.

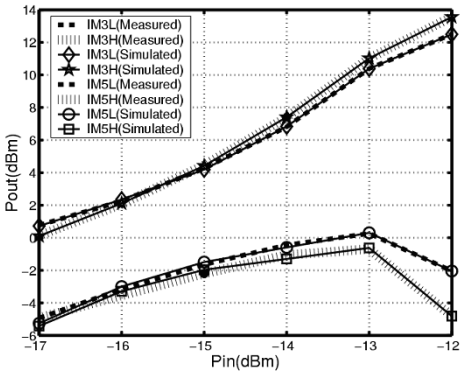

(a)

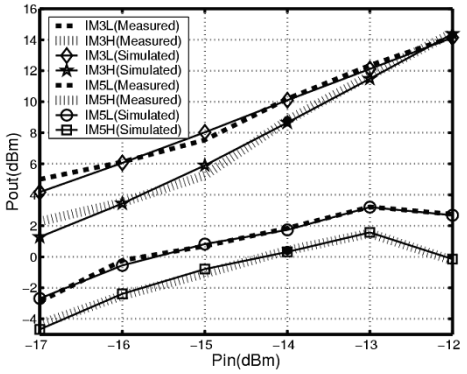

(b)

Fig. 7. Measured and simulated results for IMD3 and IMD5 asymmetries by a sweeping input power level. (a) When tone spacing is 400 kHz. (b) When tone spacing is 4.8 MHz.

where

$$\left\|\boldsymbol{E}^{(m)}\right\|_2^2 = \boldsymbol{Y}^*\boldsymbol{Y} + \hat{\boldsymbol{a}}^{(m)^*}\boldsymbol{H}^{(m)^*}\boldsymbol{H}^{(m)}\hat{\boldsymbol{a}}^{(m)} - 2\mathrm{Re}\left\{\boldsymbol{Y}^*\boldsymbol{H}^{(m)}\hat{\boldsymbol{a}}^{(m)}\right\} \quad (16)$$

where $*$ denotes the complex conjugate. From (16), the $\left\|\mathbf{E}^{(m)}\right\|_2$ term is a function of the autocorrelation of $\hat{y}^{(m)}$, and a crosscorrelation of y and $\hat{y}^{(m)}$. Here, the elements of matrix $\boldsymbol{H}^{(m)}$ are functions of the delay set $\boldsymbol{d}^{(m)}$, and $\hat{\boldsymbol{a}}^{(m)}$ is also a function of $\boldsymbol{d}^{(m)}$ from (11). Finally, the term $\|\boldsymbol{E}^{(m)}\|_2$ is a function of $\boldsymbol{d}^{(m)}$. To extract an optimal set of $\boldsymbol{d}^{(m)}$ is a difficult job, and is out of scope of this paper. However, a simplified identification method using sequential implementation that is similar with the methods proposed in [14] and [15] can be applied.

The first step is to determine $d_0^{(0)}$, which minimizes $\|\boldsymbol{E}^{(0)}\|_2^2$, by sweeping the delay tap $d_0^{(0)}$ from 0 to a maximum value of $Q_{\max}$. Usually, the derived $d_0^{(0)}$ is 0 in PA nonlinear modeling, which implies that the memoryless portion is the dominant nonlinearity in a PA. The next step is to determine the delay taps $d_j^{(1)}$ $(j = 0, 1)$. Assuming $d_0^{(1)} = d_0^{(0)}$ and sweeping delay $d_1^{(1)}$ from 0 to a maximum $Q_{\max}$, we can derive a $d_1^{(1)}$ value, which minimizes $\|\boldsymbol{E}^1\|_2^2$. Using a similar method, $d_q^{(m)}$ $(q = 0, \ldots, m)$ can be extracted. To get the optimal set $\boldsymbol{d}_{\mathrm{opt}}^{(m)}$, all $d_q^{(m)}$ terms should be recalculated. However, for simplicity, we may assume that $d_j^{(q)} = d_j^{(q-1)}$ $(j = 0, \ldots, q-1)$ and derive $d_q^{(q)}$, which minimizes $\|\boldsymbol{E}^{(q)}\|_2^2$. While this technique is not optimum in terms of the parameter space, it is efficient in terms of computational complexity.

After the model is extracted, the MER is defined as the ratio of rms error that cannot be modeled with memoryless model to the rms value of the output signal

$$\mathrm{MER} = \frac{\left\|\boldsymbol{E}^{(0)}\right\|_2}{\|\boldsymbol{Y}\|_2}. \quad (17)$$

A large value of the MER indicates that the device has a large memory effect. In the MER, if a memoryless term is a truncation form of power series, $\boldsymbol{E}^{(0)}$ includes not only the error terms from memory effects, but also the residual error terms that truncation of the memoryless model cannot capture. The improvement of the suggested model can be checked by calculating the MEMR of the predicted output when additional m branches are added to a memoryless model as follows:

$$\mathrm{MEMR}_m = 1 - \frac{\left\|\boldsymbol{E}^{(m)}\right\|_2}{\left\|\boldsymbol{E}^{(0)}\right\|_2}. \quad (18)$$

This value is 0 when memory effects are not accounted for in the device model, and is 1 when all of the memory effects are captured in the model.

TABLE I
EXTRACTED DELAYS AND PERFORMANCE (CASE 2)

	m	0	1	2	3	4
Memoryless model	MEMR	0	-	-	-	-
Memory polynomial (Unit delay)	Delay	0	1	2	3	4
	MEMR	0	0.028	0.187	0.286	0.368
Memory polynomial (Sparse delay)	Delay	0	100	70	31	52
	MEMR	0	0.124	0.276	0.367	0.428
$t_{sp} = 4.17n\,\text{sec}$, $MER = 20.02\%$, $N = 100$, $n = 7$, $Q_{\max} = 100$, $p = 6$, $r = 3$						

IV. APPLICATION TO TWO-TONE AND MULTITONE SIGNALS

A two-tone input signal $v(t)$, which has magnitude $A_i/2$ ($i = 1,\ldots,p$) and zero phase, and has tone spacings $2\omega_s$ ($s = 1,\ldots,r$) can be describes as

$$v(t) = \mathrm{Re}\Big\{\tilde{v}(t, A_i, \omega_s)e^{j\omega_c t}\Big\}. \tag{19}$$

where ω_c is the carrier frequency and ω_s is the modulation frequency ($\omega_s \ll \omega_c$). The complex envelope is

$$\tilde{v}(t, A_i, \omega_s) = \frac{A_i}{2} \cdot \left(e^{j\omega_s t} + e^{-j\omega_s t}\right). \tag{20}$$

For this input, an output signal $w(t)$ can be described as

$$w(t) = \mathrm{Re}\left[\sum_{k=-(n-1)}^{n} f_{(2k-1)}(A_i, \omega_s)e^{j(2k-1)\omega_s t}e^{j\omega_c t}\right] \tag{21}$$

where the vector $f_{(2k-1)}(A_i, \omega_s)$ can be acquired from two-tone spectrum measurements. Spectrum analyzer measurements give only magnitude information. However, if we use an extended setup as described in [16] and [17], the two-tone phase for each term can be acquired. The output complex envelope in (21) can be represented as follows:

$$\tilde{w}(t, A_i, \omega_s) = \sum_{k=-(n-1)}^{n} f_{(2k-1)}(A_i, \omega_s)e^{j(2k-1)\omega_s t}. \tag{22}$$

To get a memory polynomial model for a dynamic two-tone test signal, $\boldsymbol{Y}$ and $\boldsymbol{H}_q^{(m)}$ in Section II are redefined for two-tone dynamic signals such as

$$\boldsymbol{Y} = \begin{bmatrix} \boldsymbol{W}(A_1,\omega_1) \\ \vdots \\ \boldsymbol{W}(A_P,\omega_1) \\ \boldsymbol{W}(A_1,\omega_2) \\ \vdots \\ \boldsymbol{W}(A_P,\omega_2) \\ \vdots \\ \boldsymbol{W}(A_1,\omega_r) \\ \vdots \\ \boldsymbol{W}(A_P,\omega_r) \end{bmatrix} \quad \boldsymbol{H}_q^{(m)} = \begin{bmatrix} \boldsymbol{H}_{qT}^{(m)}(A_1,\omega_1) \\ \vdots \\ \boldsymbol{H}_{qT}^{(m)}(A_P,\omega_1) \\ \boldsymbol{H}_{qT}^{(m)}(A_1,\omega_2) \\ \vdots \\ \boldsymbol{H}_{qT}^{(m)}(A_P,\omega_2) \\ \vdots \\ \boldsymbol{H}_{qT}^{(m)}(A_1,\omega_r) \\ \vdots \\ \boldsymbol{H}_{qT}^{(m)}(A_P,\omega_r) \end{bmatrix}. \tag{23}$$

with (24) and (25), shown at the bottom of this page, and

$$h_{2k-1,q}^{(m)}[l, A_i, \omega_s] = \left|\tilde{v}\Big[l - d_q^{(m)}, A_i, \omega_s\Big]\right|^{2(k-1)} \cdot \tilde{v}\Big[l - d_q^{(m)}, A_i, \omega_s\Big] \tag{26}$$

where $\tilde{v}[l, A_i, \omega_s] = \tilde{v}(t = lt_{sp}, A_i, \omega_s)$ ($l = 1,2,\ldots,N$), $\tilde{w}[l, A_i, \omega_s] = \tilde{w}(t = lt_{sp}, A_i, \omega_s)$, and t_{sp} is the sampling period. $\boldsymbol{Y}$ is an $Npr \times 1$ vector and $\boldsymbol{H}^{(m)}$ is an $Npr \times n(m+1)$ matrix.

$$\boldsymbol{W}(A_i, \omega_s) = \Big[\tilde{w}[l, A_i, \omega_s] \quad \cdots \quad \tilde{w}[l+N-1, A_i, \omega_s]\Big]^T \tag{24}$$

$$\mathbf{H}_{qT}^{(m)}(A_i, \omega_s) = \begin{bmatrix} h_{1,q}^{(m)}[l, A_i, \omega_s] & h_{3,q}^{(m)}[l, A_i, \omega_s] & \cdots & h_{2n-1,q}^{(m)}[l, A_i, \omega_s] \\ h_{1,q}^{(m)}[l+1, A_i, \omega_s] & h_{3,q}^{(m)}[l+1, A_i, \omega_s] & \cdots & h_{2n-1,q}^{(m)}[l+1, A_i, \omega_s] \\ \vdots & \vdots & \ddots & \vdots \\ h_{1,q}^{(m)}[l+N-1, A_i, \omega_s] & h_{3,q}^{(m)}[l+N-1, A_i, \omega_s] & \cdots & h_{2n-1,q}^{(m)}[l+N-1, A_i, \omega_s] \end{bmatrix} \tag{25}$$

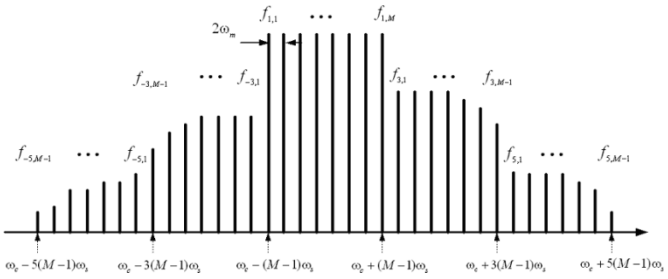

Fig. 8. Multitone nonlinear output signal in the frequency domain.

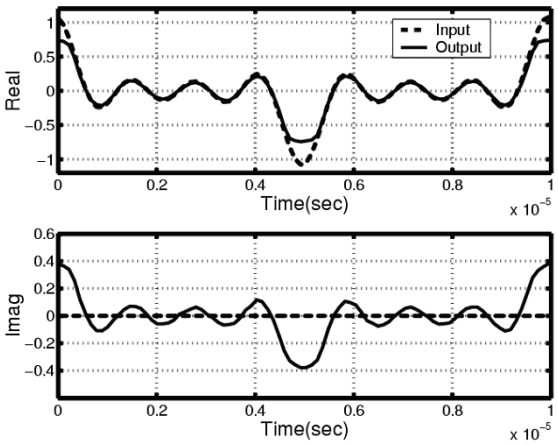

Fig. 9. Measured input and output signal in the time domain for an 880-MHz LDMOS PA with an eight-tone signal (Case 3).

Case 1: Two-Tone Output Signal With Significant Asymmetries

The output of a high-power amplifier (HPA) often shows a significant amount of asymmetry between lower and upper IMD when the PA is fed with a two-tone input signal that has symmetric lower and upper fundamental terms. To validate the proposed model, a two-tone output signal with significant asymmetries is assumed, and the PA model is extracted based on these data. To compare the simulation results and measured results in the frequency domain, the simulation procedure is summarized in Fig. 4. As shown in Fig. 5(a) and (b), third-order intermodulation distortion (IMD3) and fifth-order intermodulation distortion (IMD5) for upper terms are 10 and 15 dB, and IMD3 and IMD5 for lower terms are 20 and 25 dB. In Fig. 5(a), the simulation is executed using a memoryless model, and the results are compared. The predicted IMD3 and IMD5 give only symmetric results and the values are 14 and 19 dB. Thus, the maximum error between measured and predicted IMD in the frequency domain is 6 dB. The simulation result based on the memory polynomial is shown in Fig. 5(b). By adding one more branch to the memoryless polynomial, an asymmetric IMD is predicted exactly for both the unit delay structure and the sparse delay structure. In this case, the MEMR of the memoryless model is 0, and the MEMR of the memory polynomial model is 1.

Case 2: Real PA System With Two-Tone Dynamic Input Signal

For the experimental validation, a 2.1-GHz 170-W PEP LDMOS PA manufactured by Danam Communications Inc., San Jose, CA, was tested to investigate asymmetric IMD phenomena. A two-tone signal that has the same magnitude and phase is applied to the input, and the output lower and upper terms are measured. Fig. 6 shows the measured asymmetry results in IMD3 and IMD5 by sweeping two-tone spacings from 10 kHz to 5 MHz and by sweeping input power from -17 to -12 dBm. The difference between lower and upper fundamental terms is less than 0.2 dB so PA frequency response is not an issue. Unlike the fundamental terms, the measured IMD3 difference between upper and lower term ranges from -3 to 2 dB. The measured IMD5 difference between upper and lower term ranges from -4 to 1 dB. The amount of the asymmetry depends on the input signal power and tone spacing. The measured response was modeled with the proposed model. The measured and simulated results for IMD3 and IMD5 terms are plotted in Fig. 7(a) and (b). Fig. 7(a) is the result when two-tone spacing is 400 kHz and Fig. 7(b) is the result when two-tone spacing is 4.8 MHz. The extracted memory polynomial with sparse delay taps predicts each lower and upper term well in the wide range for two-tone spacings and the maximum error for IMD3 terms is less than 1 dB, and a simulation result is shown in Table I.

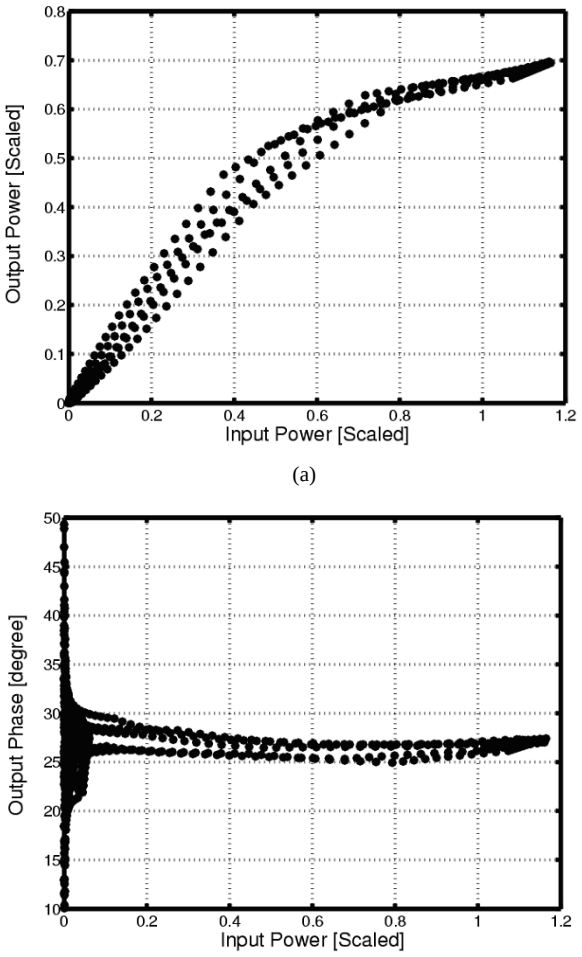

Fig. 10. Measured AM/AM and AM/PM response for an 880-MHz LDMOS PA with an eight-tone signal applied (Case 3). (a) Input power versus output power, (b) Input power versus phase difference.

TABLE II
EXTRACTED DELAYS AND PERFORMANCE (CASE 3)

	m	0	1	2	3	4
Memoryless model	MEMR	0	-	-	-	-
Memory polynomial (Unit delay)	Delay	0	1	2	3	4
	MEMR	0	0.54	0.60	0.63	0.64
Memory polynomial (Sparse delay)	Delay	0	2	84	82	59
	MEMR	0	0.57	0.62	0.66	0.68
$t_{sp} = 56n$ sec, $MER = 5.62\%$, $N = 100$, $n = 3$, $Q_{max} = 100$, $p = 1$, $r = 1$						

The same method as described above for two-tone signals can be applied to multitone signals. The M-tone real bandpass signal, which has the center frequency ω_c $(= 2\pi f_c)$ and the tone spacing $2\omega_s$ can be described as

$$v(t) = \sum_{i=1}^{M} A_i \cos\left[\left(\omega_c + (2i - M - 1)\omega_s\right)t + \theta_i\right]. \quad (27)$$

By simple calculation, the complex envelope signal $\tilde{v}(t)$ can be acquired

$$\tilde{v}(t) = \sum_{i=1}^{M} c_i e^{j(2i-M-1)\omega_s t}. \quad (28)$$

where $c_i = A_i e^{j\theta_i}$.

Considering nonlinear terms up to $2n-1$ order, the output signal is a multitone signal, which has $(2n-1)\times(M-1)+1$ terms, as shown in Fig. 8. The output complex envelope signal can be described as

$$\tilde{w}(t) = \sum_{i=1}^{M} f_{1,i} \exp\left[j(2i - M - 1)\omega_s t\right] + \sum_{\substack{k=-(n-1) \\ k\neq 0}}^{n-1} \sum_{i=1}^{M-1} f_{\mathrm{sgn}(k)\cdot(2|k|+1),i} \cdot \exp\left[j\mathrm{sgn}(k)\cdot\left((2k-1)\cdot(M-1)+2i\right)\omega_s t\right]. \quad (29)$$

Using the extracted complex envelope signals for input and output of multitone signals, the memory polynomial model for a measured multitone signal can also be extracted.

Case 3: Real PA System With Eight-Tone Input Signal

For the experimental validation, an 880-MHz 170-W PEP LDMOS PA manufactured by Danam Communications Inc. was tested to investigate dynamic AM/AM and AM/PM using an eight-tone signal. The input signal is an eight-tone signal with 200-kHz tone spacings for each adjacent tone, and the magnitude and phase are the same for each tone. For this signal with aligned phases, the eight-tone signal has a maximum crest factor of approximately 9 dB. The output of the PA signal is down-converted and in-channel (I) and quadrature (Q) channel signals are measured in a vector signal analyzer (VSA). The measured I and Q channel time-domain data are shown in Fig. 9. The AM/AM response and AM/PM response show a hysteresis depending on the history of past input signals, as shown in Fig. 10. The measured eight-tone data is modeled with a memoryless model and a model based on a memory polynomial, and the results are compared in Table II.

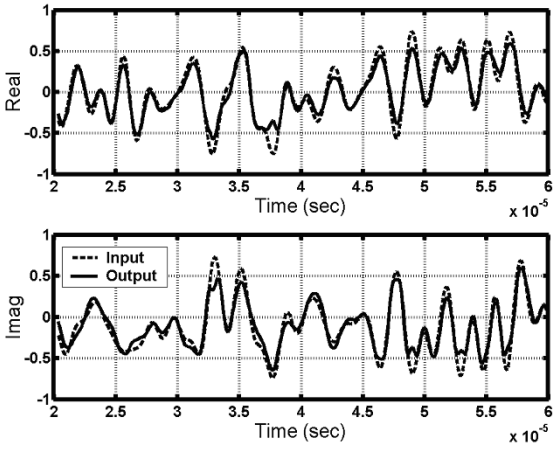

Fig. 11. Simulated input and output signal in the time domain for a simulated sparse model with an IS-95B signal (Case 4).

V. APPLICATION TO DIGITALLY MODULATED SIGNALS

In this section, two more cases are studied for a digitally modulated signal to validate the proposed model. An IS-95B CDMA signal is used to extract a model and compare the simulated result with a measured result. The sampling frequency to capture the signal is $f_{sp} = 9.83$ MHz. For both cases, the memory polynomial model with unit and with sparse delays in Section II are applied to estimate the system parameter from input and output data.

Case 4: Simulated Sparse System With IS-95B Input Signal

Here, we generate a PA model that is a sparse system that has a transfer function with the form described in (3) with $m = 3$ and $n = 2$.

The parameters of the given system are as follows:

$$\begin{aligned} a_{1,0} &= 0.98 - 0.3i \quad a_{3,0} = -0.3 + 0.42i \quad d_0 = 0 \\ a_{1,1} &= 0.06 + 0.03i \quad a_{3,1} = -0.02 + 0.05i \quad d_1 = 10 \\ a_{1,2} &= 0.02 + 0.08i \quad a_{3,2} = -0.01 - 0.08i \quad d_2 = 100 \\ a_{1,3} &= -0.01 + 0.02i \quad a_{3,3} = 0.02 - 0.01i \quad d_3 = 50. \end{aligned} \quad (30)$$

For this given system, an output signal is derived. The input and output signals in the time domain are shown in Fig. 11. The

TABLE III
EXTRACTED DELAYS, COEFFICIENTS, AND PERFORMANCE (CASE 4)

	m	Delay	Extracted Coefficients	MEMR
Memoryless Model	0	0	$\hat{a}_{1,0} = 0.9798 - 0.2887i$, $\hat{a}_{3,0} = -0.2901 + 0.4350i$	0
Memory polynomial (Unit delay)	0	0	$\hat{a}_{1,0} = 0.9798 - 0.2887i$, $\hat{a}_{3,0} = -0.2901 + 0.4350i$	0
	1	1	$\hat{a}_{1,0} = 0.7969 - 0.4685i$, $\hat{a}_{1,1} = 0.2142 + 0.1832i$, $\hat{a}_{3,0} = -0.2340 + 0.4487i$, $\hat{a}_{3,1} = -0.0527 - 0.0203i$,	0.11
	2	2	$\hat{a}_{1,0} = 1.4045 + 0.8149i$, $\hat{a}_{1,1} = -1.0554 - 2.3300i$, $\hat{a}_{1,2} = 0.6497 + 1.2759i$, $\hat{a}_{3,0} = -0.2484 + 0.3705i$, $\hat{a}_{3,1} = -0.0517 + 0.0896i$, $\hat{a}_{3,2} = 0.0289 - 0.0404i$,	0.32
	3	3	$\hat{a}_{1,0} = 0.7411 - 0.0234i$, $\hat{a}_{1,1} = 0.9881 + 0.2705i$, $\hat{a}_{1,2} = -1.5036 - 1.4375i$, $\hat{a}_{1,3} = 0.7795 + 0.9569i$, $\hat{a}_{3,0} = -0.1113 + 0.0639i$, $\hat{a}_{3,1} = -0.4341 + 0.9413i$, $\hat{a}_{3,2} = 0.3988 - 0.9229i$, $\hat{a}_{3,3} = -0.1281 + 0.3353i$	0.38
Memory polynomial (Sparse delay)	0	0	$\hat{a}_{1,0} = 0.9798 - 0.2887i$, $\hat{a}_{3,0} = -0.2901 + 0.4350i$	0
	1	10	$\hat{a}_{1,0} = 0.9859 - 0.2856i$, $\hat{a}_{1,1} = 0.0565 + 0.0367i$, $\hat{a}_{3,0} = -0.2997 + 0.4138i$, $\hat{a}_{3,1} = -0.0109 + 0.0508i$,	0.50
	2	100	$\hat{a}_{1,0} = 0.9774 - 0.3017i$, $\hat{a}_{1,1} = 0.0646 + 0.0349i$, $\hat{a}_{1,2} = 0.0157 + 0.0793i$, $\hat{a}_{3,0} = -0.2929 + 0.4199i$, $\hat{a}_{3,1} = -0.0230 + 0.0460i$, $\hat{a}_{3,2} = 0.0002 - 0.0739i$,	0.84
	3	50	$\hat{a}_{1,0} = 0.9800 - 0.3000i$, $\hat{a}_{1,1} = 0.0600 + 0.0300i$, $\hat{a}_{1,2} = 0.0200 + 0.0800i$, $\hat{a}_{1,3} = -0.0100 + 0.0200i$, $\hat{a}_{3,0} = -0.3000 + 0.4200i$, $\hat{a}_{3,1} = -0.0200 + 0.0500i$, $\hat{a}_{3,2} = -0.0100 - 0.0800i$, $\hat{a}_{3,3} = 0.0200 - 0.0100i$	1.00
$t_{sp} = 102n\,\text{sec}$, $MER = 11.65\%$, $N = 200$, $n = 2$, $Q_{\max} = 200$				

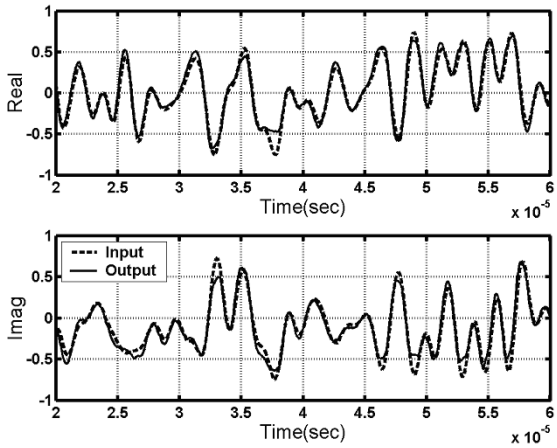

Fig. 12. Measured input and output signal in the time domain for an 880-MHz LDMOS PA with an IS-95B signal (Case 5).

AM/AM and AM/PM show dispersion in the relationships between input and output signals because the output depends on current and past input signals. By adding the delay branches up to four, the system is estimated based on input and output data. The extracted coefficients, delays, and MEMR values are shown in Table III. The MEMR increases as m increases, which means the performance of modeling memory effects increases. If a memory polynomial model with sparse delay taps is used, the exact model can be derived, and the MEMR is 1 when $m = 3$. In this case, the performance of a memory polynomial with sparse delay is much better compared to that of a memory polynomial with unit delay, which has an MEMR of 0.38.

Case 5: PA System With IS-95B Input Signal

For the experimental validation, IS-95B time-domain input and output data are measured for the 880-MHz LDMOS HPA system. The IS-95B baseband signal is generated and up-converted to RF signal using an arbitrary signal generator. The bandpass input is fed into an HPA. The output signal of the HPA is down-converted, and its time domain I and Q channel data are captured using an Agilent 89410 VSA. The measured I and Q data are plotted in Fig. 12. The AM/AM and AM/PM characteristics from the measured time data are plotted in Fig. 13. For this

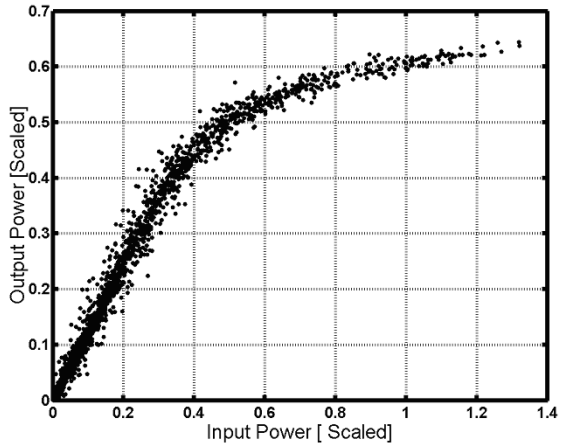

(a)

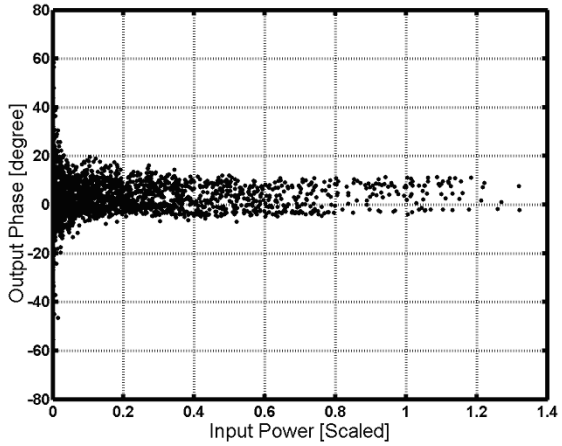

(b)

Fig. 13. AM/AM and AM/PM response for an 880-MHz LDMOS PA with an IS-95B signal (Case 5). (a) Input power versus output power. (b) Input power versus phase difference.

TABLE IV
EXTRACTED DELAYS AND PERFORMANCE (CASE 5)

	m	0	1	2	3	4
Memoryless model	MEMR	0	-	-	-	-
Memory polynomial (Unit delay)	Delay	0	1	2	3	4
	MEMR	0	0.55	0.59	0.60	0.60
Memory polynomial (Sparse delay)	Delay	0	1	3	37	98
	MEMR	0	0.55	0.59	0.62	0.64
$t_{sp} = 102n\,\text{sec}$, $MER = 8.89\%$, $N = 200$, $n = 2$, $Q_{\max} = 200$						

measured signal, the parameters of the proposed model are extracted. The third-order nonlinearity is considered and the maximum memory depth considered in modeling is 200 samples, which corresponds to 20 μs. The first dominant delay tap, which minimizes error, is zero. This implies that the memoryless portion is dominant. The extracted consecutive sparse delay values are shown in Table IV. To compare error reduction of the proposed model, the MEMR values are calculated and compared in Table IV. When m is four, the memory polynomial model with sparse delay taps gives 4% better performance compared to that of the model with unit delay taps. We conclude that the small amount of improvement compared to that of case 4 is due to widely distributed range of delays in the physical PA.

VI. CONCLUSIONS

In this paper, we have shown that a PA behavioral model based on the memory polynomial can improve the accuracy in predicting output nonlinear signals by modeling memory effects. To obtain better performance in rms error reduction, an extended structure based on sparse taps was developed and is the primary contribution of this study. The proposed model can be used to simulate such phenomena as asymmetric IMD, and dynamic AM/AM and AM/PM that depend on the history of past input power levels.

To validate the proposed modeling technique, many cases are studied. In case 1, the asymmetric two-tone output was modeled and compared with the measured output. Memoryless models cannot model the asymmetric phenomena, but the proposed model predicts IMD asymmetries accurately by adding an additional branch to the memoryless polynomial. In case 2, a two-tone output with asymmetries is measured by sweeping input power and tone spacing for a 2.1-GHz LDMOS PA. The predicted results show the maximum error for the IMD3 term is within 1 dB in the measured range. In case 3, an 880-MHz LDMOS PA was measured with an eight-tone signal and modeled with a proposed method. The simulation results show that the MEMR is 4% better when a sparse structure was used with $m = 4$. In case 4, a sparse structure model is assumed and modeled. In this case, the performance improvement of the memory polynomial with a sparse structure was significant. In case 5, an 880-MHz LDMOS PA is measured with an IS-95B signal and modeled with a proposed method. In this case, the MEMR of a model based on sparse tap with $m = 4$ is 4% better compared to that of the unit delay structure.

ACKNOWLEDGMENT

The authors wish to thank Y. Park, L. Ding, and Prof. G. T. Zhou, all of the Georgia Institute of Technology, Atlanta, for their helpful comments and supports in the development and validation of this model.

REFERENCES

[1] S. C. Cripps, *Advanced Techniques in RF Power Amplifier Design*. Norwood, MA: Artech House, 2002.
[2] N. B. Carvalho and J. C. Pedro, "A comprehensive explanation of distortion sideband asymmetries," *IEEE Trans. Microwave Theory Tech.*, vol. 50, pp. 2090–2101, Sept. 2002.
[3] J. Vuolevi, T. Rahkonen, and J. Manninen, "Measurement technique for characterizing memory effects in RF power amplifiers," *IEEE Trans. Microwave Theory Tech.*, vol. 49, pp. 1383–1389, Aug. 2001.
[4] D. J. Williams, J. Leckey, and P. J. Tasker, "A study of the effect of envelope impedance on intermodulation asymmetry using a two-tone time domain measurement system," in *IEEE MTT-S Int. Microwave Symp. Dig.*, Seattle, WA, June 2002, pp. 1841–1844.
[5] H. Ku, M. McKinley, and J. S. Kenney, "Quantifying memory effects in RF power amplifiers," *IEEE Trans. Microwave Theory Tech.*, vol. 50, pp. 2843–2849, Dec. 2002.
[6] W. Bosch and G. Gatti, "Measurement and simulation of memory effects in predistortion linearizers," *IEEE Trans. Microwave Theory Tech.*, vol. 37, pp. 1885–1890, Dec. 1989.
[7] A. A. Moulthrop, C. J. Clark, C. P. Silva, and M. S. Muha, "A dynamic AM/AM and AM/PM measurement technique," in *IEEE MTT-S Int. Microwave Symp. Dig.*, vol. 3, June 1997, pp. 1455–1458.
[8] P. M. Asbeck, H. Kobayashi, M. Iwamoto, G. Hanington, S. Nam, and L. E. Larson, "Augmented behavioral characterization for modeling the nonlinear response of power amplifiers," in *IEEE MTT-S Int. Microwave Symp. Dig.*, Seattle, WA, June 2002, pp. 135–138.
[9] A. A. Saleh, "Frequency-independent and frequency-dependent nonlinear models of TWT amplifiers," *IEEE Trans. Commun.*, vol. COM-29, pp. 1715–1720, Nov. 1981.
[10] M. S. Muha, C. J. Clark, A. A. Moulthrop, and C. P. Silva, "Validation of power amplifier nonlinear block models," in *IEEE MTT-S Int. Microwave Symp. Dig.*, Anaheim, CA, June 14–17, 1999, pp. 759–762.
[11] C. J. Clark, C. P. Silva, A. A. Moulthrop, and M. S. Muha, "Power-amplifier characterization using a two-tone measurement technique," *IEEE Trans. Microwave Theory Tech.*, vol. 50, pp. 1590–1602, June 2002.
[12] J. Kim and K. Konstantinou, "Digital predistortion of wideband signals based on power amplifier model with memory," *Electron. Lett.*, vol. 37, no. 23, pp. 1417–1418, Nov. 2001.
[13] L. Ding, G. T. Zhou, D. R. Morgan, Z. Ma, J. S. Kenney, J. Kim, and C. R. Giardina, "Memory polynomial predistorter based on the indirect learning architecture," in *Proc. IEEE Global Telecomm. Conf.*, Taipei, Taiwan, R.O.C., Nov. 2002, pp. 967–971.
[14] D. M. Etter and Y. Cheng, "System modeling using an adaptive delay filter," *IEEE Trans. Circuits Syst.*, vol. CAS-34, pp. 770–774, July 1987.
[15] Y. Cheng and D. M. Etter, "Analysis of an adaptive technique for modeling sparse systems," *IEEE Trans. Acoust., Speech, Signal Processing*, vol. 37, pp. 254–264, Feb. 1989.
[16] N. Suematsu, Y. Iyama, and O. Ishida, "Transfer characteristic of IM3 relative phase for a GaAs FET amplifier," *IEEE Trans. Microwave Theory Tech.*, vol. 45, pp. 2509–2514, Dec. 1997.
[17] Y. Yang, J. Yi, J. Nam, B. Kim, and M. Park, "Measurement of two-tone transfer characteristics of high-power amplifiers," *IEEE Trans. Microwave Theory Tech.*, vol. 49, pp. 568–571, Mar. 2001.

Hyunchul Ku (S'00) was born in Pusan, Korea, in 1972. He received the B.S. (with honors) and M.S. degrees in electrical engineering from the Seoul National University, Seoul, Korea, in 1995 and 1997, respectively, and is currently working toward the Ph.D. degree in electrical and computer engineering at the Georgia Institute of Technology, Atlanta.

From 1997 to 1999, he was a Member of Technical Staff with the Wireless Research Center, Korea Telecom (KT), Seoul, Korea. His current research interests include behavioral modeling and characterization of RF devices, PA linearization, and statistical signal processing.

J. Stevenson Kenney (S'84–M'85–SM'01) was born in St. Louis, MO, in 1962. He received the B.S.E.E. (with honors), M.S.E.E., and Ph.D. degrees in electrical engineering from the Georgia Institute of Technology, Atlanta, in 1985, 1990, and 1994, respectively.

In January 2000, he joined the faculty of the Georgia Institute of Technology, where he is currently an Associate Professor of electrical and computer engineering. He currently teaches and conducts research in the areas of power-amplifier linearization, smart antenna design, and RF integrated circuit (RFIC) design. He possesses over 14 years of industrial experience in wireless communications. He has held engineering and management positions with Electromagnetic Sciences, Scientific Atlanta, and Pacific Monolithics. Prior to rejoining the Georgia Institute of Technology, he was Director of Engineering with the Spectrian Corporation, Sunnyvale, CA. He has authored or coauthored over 50 technical papers, conference papers, and workshop presentations in the areas of acoustics, microelectronics, microwave design, and telecommunications.

Dr. Kenney has been an active member of the IEEE Microwave Theory and Techniques Society (IEEE MTT-S) for 20 years. He served as an officer on the Santa Clara Valley chapter of the IEEE MTT-S from 1996 to 2000. He is currently serving his second term on the IEEE MTT-S Administrative Committee (AdCom), and was the treasurer for 2001 and 2002. He served on the IEEE MTT-S International Microwave Symposium (IMS) Steering Committee in 1993 and 1996. He serves on the IEEE MTT-S Technical Committee. He was the Technical Program Committee co-chair for the 2002 Radio and Wireless Conference (RAWCON). He currently serves as the general co-chair for the 2003 RAWCON. He has served on the Editorial Board for the IEEE TRANSACTIONS ON MICROWAVE THEORY AND TECHNIQUES AND THE IEEE MICROWAVE AND WIRELESS COMPONENTS LETTERS. He is currently co-chair of the RF Components Technical Interest Group of the National Electronics Manufacturing Initiative.